Accepted for publication in the Astrophysical Journal Letters
Preprint typeset using LaTeX style emulateapj v. 03/07/07

SEARCHING FOR NEEDLES IN HAYSTACKS - USING THE *FERMI*/GBM TO FIND GRB $\gamma-$RAYS WITH THE *FERMI*/LAT DETECTOR

C. W. Akerlof[1], W. Zheng[1], S. B. Pandey[1,2], T. A. McKay[1]

Accepted for publication in the Astrophysical Journal Letters

ABSTRACT

From the launch of the Fermi Gamma-ray Space Telescope to July 9, 2010, the Gamma-ray Burst Monitor (GBM) has detected 497 probable GRB events. Twenty-two of these satisfy the simultaneous requirements of an estimated burst direction within 52° of the Fermi Large Area Telescope (LAT) boresight and a low energy fluence exceeding 5 μerg/cm^2. Using matched filter techniques, the spatially correlated *Fermi*/LAT photon data above 100 MeV have been examined for evidence of bursts that have so far evaded detection at these energies. High energy emission is detected with great confidence for one event, GRB 090228A. Since the LAT has significantly better angular resolution than the GBM, real-time application of these methods could open the door to optical identification and richer characterization of a larger fraction of the relatively rare GRBs that include high energy emission.

Subject headings: Gamma-ray burst: general

1. INTRODUCTION

One of the more surprising results of the Compton Gamma-Ray Observatory (CGRO) was the EGRET discovery of an 18 GeV photon associated with GRB 940217 (Hurley 1994). About a half-dozen bursts were seen over the course of the CGRO mission with photons above 100 MeV (Catelli 1998, Dingus 2003). Since the GRB spectral energy distribution at lower energies has been well characterized by a modified power law with peak fluxes at energies of the order of 200 KeV, the existence of photons at energies 10^4 times higher puts a significant constraint on any viable model of the GRB phenomenon. This has been a subject of great interest for missions that followed EGRET. Prior to launch of the Fermi Gamma-ray Space Telescope, it was possible to speculate that the LAT instrument would detect more than 200 GRB events per year (Dingus, 2003). In the two year period since the launch of the Fermi Gamma-ray Space Telescope, the Gamma-ray Burst Monitor (GBM) has reported approximately 475 GRBs, ie. a rate of about 250 per year. Over essentially the same period, only 17 bursts have been identified by the Fermi/LAT. We now see that the range of GRB photon energies extends over a scale of 10^6 but the physical dynamics of these phenomena are still not understood. This is coupled to the question of whether high energy photons are associated with all GRBs or only with a small sub-class. Since the Fermi mission is unlikely to be duplicated any time soon, there is some urgency to assuring that the maximum information is being extracted from this valuable facility. Thus, our group has set about developing techniques for enlarging the number of gamma-ray bursts identified with high energy photon emission, ie. above 100 MeV.

The first result of this effort has established the correlation of two *Swift*/XRT-localized bursts, GRB 080905A and GRB 091208B, with high energy photons in the *Fermi*/LAT detector (Akerlof el al. (2010), hereafter A10). The statistical technique employed is the *matched filter* method, most familiar to those detecting signals in the time domain. The underlying assumption is that the characteristics of both the signal and background are *a priori* known functions of one or more variables. Since the matched filter maximizes the signal-to-noise ratio, moderate departures from optimality degrade the filter performance relatively slowly, making this a valuable tool for investigating the possible existence of faint signals. The details of the filter algorithm are explicitly described in A10. In this paper, we take the next harder step of dropping our reliance on precision burst coordinates provided by Swift or other similar high resolution instruments. Instead, we use the approximate localization of the *Fermi*/GBM to map a region of interest on the *Fermi*/LAT field of view. By identifying high energy photon clusters, provisional burst coordinates can be determined with significantly smaller errors than available from the GBM. From there, the burst identification follows along lines set out in A10.

2. SAMPLE SELECTION

As a first step in this program, a list of all GBM triggers was obtained from the *fermigbrst* catalog maintained by the *Fermi* Science Support Center[3]. The catalog contains 497 GRB triggers from launch to July 9, 2010. This list was cross-matched with Table 1 in Guetta & Pian (2009) and Table 2 in Guetta et al. (2010) to identify the burst GCN designations and the low energy fluences. For triggers occuring after February 18, 2010, fluences were obtained from individual GCN circulars. GBM triggers were also checked against XRT locations from *Swift*[4] to remove events already considered in A10.

Using data from the Fermi spacecraft attitude file, we further selected those triggers with a boresight angle less than 52° and an estimated GBM error circle less than 10°. Events without GBM fluence information or previously claimed LAT detections[5] were also discarded. Ap-

[1] Randall Laboratory of Physics, Univ. of Michigan, 450 Church Street, Ann Arbor, MI, 48109-1040, USA
[2] Aryabhatta Research Institute of Observational Sciences, Manora Peak, Nainital, India, 263129

[3] http://heasarc.gsfc.nasa.gov/W3Browse/fermi/fermigbrst.html
[4] http://heasarc.gsfc.nasa.gov/docs/swift/archive/grb_table/
[5] http://fermi.gsfc.nasa.gov/ssc/observations/types/grbs/grb_table/

TABLE 1
List of 22 GBM trigger GRBs

GRB	Trigger	RA (°)	Dec (°)	S_{GBM} μerg/cm^2
080830	080830368	160.10	30.80	9.2
080904	080904886	214.20	-30.30	5.0
080906B	080906212	182.80	-6.40	10.9
080925	080925775	96.10	18.20	19.4
081122A	081122520	339.10	40.00	9.6
081231	081231140	208.60	-35.80	12.0
090112A	090112332	110.90	-30.40	5.2
090131	090131090	352.30	21.20	22.3
090227A	090227310	3.30	-43.00	9.0
090228A	090228204	106.80	-24.30	6.1
090319	090319622	283.30	-8.90	7.5
090330	090330279	160.20	-8.20	11.4
090514	090514006	12.30	-10.90	8.1
090516B	090516137	122.20	-71.62	30.0
090829A	090829672	329.23	-34.19	102.0
090829B	090829702	354.99	-9.36	6.4
090922A	090922539	17.16	74.30	11.4
091120	091120191	226.81	-21.79	30.2
100122A	100122616	79.20	-2.71	10.0
100131A	100131730	120.40	16.45	7.7
100423B	100423244	119.67	5.78	12.3
100511A	100511035	109.29	-4.65	7.1

plying a final cut on GBM fluence (8 - 1000 KeV) requiring greater than 5.0 μerg/cm^2 reduced the number to 22 events (see Table 1). These are termed the "GBM" data. 464 additional fields were taken at random on the sky with similar criteria to study the background behavior and are identified as the"random" data in the following text.

3. SIGNAL DETECTION TECHNIQUE

The core task of this search procedure is the identification of triplet clusters of photons in the *Fermi*/LAT instrument whose spatial accuracy is considerably better than the GBM. The set of photon data for each candidate burst is confined to lie within a 16° cone angle of the GBM direction and a time window extending from zero to 47.5 s after the GBM burst trigger. The procedure first computes a signal weight for each photon pair based on photon energy, detection time, photon event class and angular separation relative to the expected LAT PSF errors. The photon pair weights are subject to a weak threshold cut designed to avoid combinatorial overload should large photon numbers be encountered. In practice, this was not a severe problem and can be ignored. The formula for the pair weights is given by:

$$Q_{ij} = w_i \cdot w_j \cdot \Delta_{ij}, \tag{1}$$

where

$$w_i = w_E(i) \cdot w_t(i) \cdot w_c(i) \cdot 4\pi\sigma^2_{PSF}(E_i), \tag{2}$$

$$\Delta_{ij} = \frac{e^{-\delta_{ij}}}{4\pi(\sigma^2_{PSF}(E_i) + \sigma^2_{PSF}(E_j))}, \tag{3}$$

$$\delta_{ij} = \frac{1}{2}\frac{\theta^2_{ij}}{\sigma^2_{PSF}(E_i) + \sigma^2_{PSF}(E_j)}, \tag{4}$$

and θ_{ij} is the angle between the i'th and j'th photon. The definitions of w_E, w_t and w_c can be found in equation 1,3 and 4 of A10.

The next step is to link photon pairs so that the three pairs, {i, j}, {j, k} and {i, k}, become identified as the triplet, {i, j, k}. The triplet weight value is computed by the formula:

$$R_{ijk} = (w_i \cdot w_j \cdot w_k \cdot \Delta_{ij} \cdot \Delta_{jk} \cdot \Delta_{ik})^{\frac{1}{3}} \tag{5}$$

The triplet weights are ranked by value and the set is pruned by the condition that a triplet element, R_{ilm}, is removed if $R_{ilm} < R_{ijk}$. This leaves a set of triplet clusters, each with a discrete complement of three photons. For each of these clusters, a PSF-weighted estimate of the burst direction is performed and the matched filter angle weight, w_θ is computed with respect to this vector as described in equation 2 of A10. At this point, an event weight for each cluster is computed by the formulas given in A10 with one small modification. In the scheme described here, the GRB direction is not initially defined with any precision. Thus, it is inappropriate to include a $1/\sigma^2_{PSF}$ factor for all values of w_E. For the highest energy photon in each triplet, the $4\pi\sigma^2_{PSF}$ factor is removed to reflect that this leading photon plays the principal role in fixing the apparent GRB direction. Although the calculations carry each cluster through the same computational path, the expectation is that the cluster with the highest matched filter weight is the most probable identification.

The 22 GBM fields described earlier were the target of this investigation. We recognized that the most convincing argument for a true LAT identification should rely on the statistical distributions for the matched filter weights in LAT fields with similar characteristics. To increase that number as much as possible, the LAT fields of view were segmented into 12 circular tiles embedded on a spherical surface. Each tile subtends a cone with a half-angle of 16.0°. This tiling scheme was applied to both the GBM and random field data sets to realize 182 and 3440 independent directions in space satisfying all the criteria described previously. Taking advantage of the fact that each field observation was blocked into a 250-s segment, the number of independent observations was multiplied by five by regarding each 50-s time slice as a separate sample. Thus, there are 910 background measurements taken from LAT observations obtained simultaneously with the candidate GBM fields and an additional 17200 samples taken under similar but not identical conditions. One particular concern for an analysis of this type is that false positives will selectively occur as the sample photon rate rises substantially above the mean. Evidence that this is not the case here is shown in Figure 1 which plots the cumulative distribution of the total number of photons within the LAT field of view over a 250-s interval. These rates explicitly exclude contamination from photons beyond the 105° zenith angle cut. As shown in the plot, the prominent GBM trigger event reported here is not associated specifically with fields with high ambient background rates. The similarity of the distributions for GBM and random fields also shows that the GBM data are not pathological as far as rates are concerned.

4. RESULTS

Our statistical localization and weighting scheme identified one outstanding candidate for high energy photon emission, GRB 090228A. The best estimate for the probability of such an occurence by chance alone was obtained by performing identical searches on random LAT fields with the same criteria. Thus, 11 out of 17200 random fields generated matched filter weights exceeding the

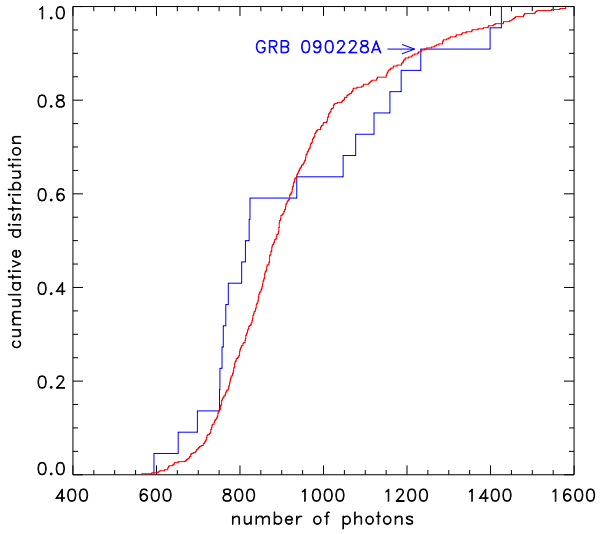

FIG. 1.— Cumulative distributions of LAT photon rates over 250-s intervals for the GBM (blue) and random background (red) fields. These rates reflect the entire LAT FoV except for photons that lie outside the 105° zenith angle cut. The rate corresponding to the most prominent GBM event is indicated by the arrow.

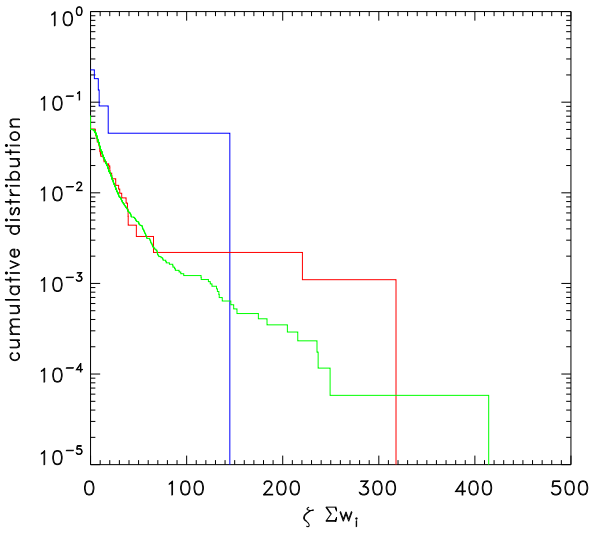

FIG. 2.— Complements of the cumulative distributions for $\zeta\sum w_i$ for 22 GBM fields (blue), 910 random fields obtained nearly simultaneously with the GBM data (red) and 17200 random fields obtained at random times (green).

value for our candidate event. Multiplying by a trials factor of 22 for the number of GBM localized fields considered yields a false positive probability of 1.4%. To check that these correlations were simply not due to preferentially higher background rates for the GBM exposures, we also performed similar calculations for the LAT data confined to an average of 8 uncorrelated directions per exposure and five independent time intervals from the same GBM data sets. In this case, 2 fields out of 910 exceed the candidate signal for a false positive rate of 4.8%. The cumulative distributions are plotted in Figure 2. The statistical similarity of the GBM off-axis and random field data demonstrates that the GBM data set is not correlated with anomalous environmental conditions such as higher cosmic ray background rates. A list of photons associated with this burst is provided in Table 2.

The GBM data for GRB 090228A is described in GCN 8918 (von Kienlin, et al., 2009). According to this note, the burst was localized to a $1-\sigma$ accuracy of better than 1° with an additional systematic uncertainty of the order of 2.5°. The coordinate values obtained by the GBM group and this analysis are listed in Table 2. The GBM value generated some concern since our cluster finder position disagreed by 8.7°. Fortuitously as this manuscript was being drafted, a paper was posted to astro-ph (Guiriec et al., 2010) providing a burst direction with an estimated accuracy of 0.2° and lying 0.5° from our own estimate. We believe that this establishes the validity of our identification to near certainty. In addition, the positive GRB correlation of Event Class 2 and 3 photon rates discussed in A10 was observed for the ensemble of GBM fields as well. The photon clustering is easily observed in the sky map shown in Figure 3.

5. DISCUSSION

The one event identified in this paper establishes the validity of our statistical techniques to a level of near certainty. By using GBM triggers to guide the discovery of photon clusters in the LAT, the phase space for finding counterparts can be reduced from hundreds of square degrees to one square degree or less. This makes a very significant difference for those seeking to identify GRB optical counterparts. If the algorithms used here could be adapted to the real time environment, the number of bursts with high energy associations could be increased appreciably. The additional computational load is negligible - about 30 ms per day. For such real time applications, the high selectivity employed here is overkill - any identification that can be corroborated optically will suffice. Thus, effective signal-to-noise rates of the order of

TABLE 2
GRB 090228A HIGH ENERGY PHOTON LIST AND CELESTIAL COORDINATE ESTIMATES

i	t (s)	θ (°)	E (MeV)	c	w_i
1	2.007	1.692	125.241	2	52.814
2	3.752	2.611	206.983	3	46.545
3	25.141	0.592	308.638	3	44.278
4	3.243	1.978	638.692	3	1.356
5	4.966	0.063	2787.028	3	*0.376
6	33.621	5.063	340.623	1	0.002

$\zeta = 0.99722$ $\zeta\sum w_i = 144.969$

source	α (°)	δ (°)	σ_θ (°)	$\theta^d_{i-1,i}$ (°)
GBM[a]	106.80	-24.30	$\lesssim 3.0$	
LAT[b]	98.56	-28.86	0.18	8.66
IPN[c]	98.30	-28.40	0.02	0.51

* indicates diminished w_E for highest energy photon
[a] von Kienlin et al. (2009)
[b] this paper
[c] Guiriec et al. (2010)
[d] $\theta_{i-1,i}$ is the angle between the spatial directions for the GBM and LAT or the LAT and IPN

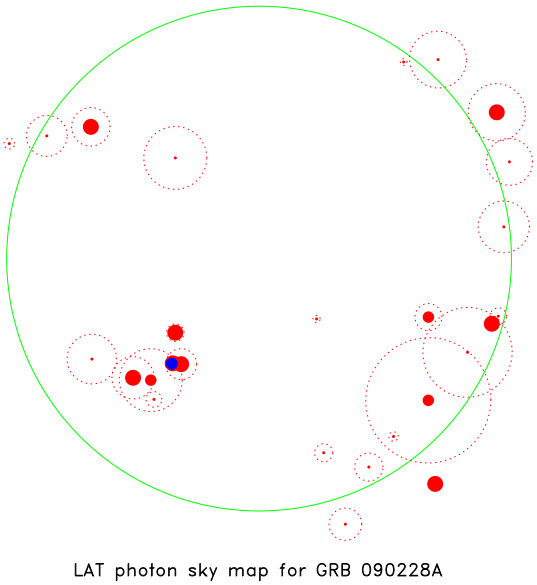

FIG. 3.— Sky map of > 100 MeV photons for GRB 090228A. The diameter of each dot is proportional to its statistical weight. Thus, the largest diameters represent Event Class 3, etc. The dotted circles around each point indicate the $1-\sigma$ errors. The figure is centered on the nominal coordinates furnished by the GBM; the blue dot on the lower left shows the GRB coordinates computed by the cluster algorithm described in the text. The large green circle depicts the boundaries of the 16.0° cone that defines the fiducial boundaries for the cluster search. North is up and East is to the right.

unity are extremely valuable. As shown here, these techniques greatly enhance the dynamic range over which high energy radiation can be explored. It is not too outrageous to claim that this is the equivalent of making the LAT three to ten times larger in size.

As was noted in A10, the most surprising aspect of our recent work is the very small number of GRBs that can be positively identified with high energy emission despite the substantially lower fluence thresholds. This is a mystery which deserves serious consideration. We hope that raising new questions is sometimes more useful than answering old problems.

We thank Chris Shrader, director of the *Fermi* Science Support Center for his considerable help in obtaining and interpreting the *Fermi* mission data products. Fang Yuan provided valuable assistance in the initial process of learning how to access and manipulate the *Fermi* data. This research is supported by NASA grant NNX08AV63G and NSF grant PHY-0801007.

REFERENCES

Akerlof, C. W., et al., 2010, ApJ, in press, (arXiv:1010.1436v2 [astro-ph.HE])
Catelli, J. R., Dingus, B. L. & Schneid, E. J., 1998, AIP Conf. Proc., 428, 309
Dingus, B. L., 2003, AIP Conf. Proc., 662, 240
Guetta, D., & Pian, E., 2009, arXiv:0910.2134v2 [astro-ph.HE]
Guetta, D., et al., 2010, arXiv:1003.0566v2 [astro-ph.HE]
Guiriec, S., et al., 2010, arXiv:1009.5045v2 [astro-ph.HE]
Hurley, K., et al., 1994, Nature, 372, 652
von Kienlin, A. et al., 2009, GCN Circ., 8918